Synthesis of linked carbon monolayers: Films, balloons, tubes, and pleated sheets

Mitchell J. Schultz*†, Xiaoyu Zhang*‡, Sakulsuk Unarunotai*†, Dahl-Young Khang*‡, Qing Cao*†, Congjun Wang*‡, Changhui Lei*‡, Scott MacLaren*‡, Julio A. N. T. Soares*†, Ivan Petrov*‡, Jeffrey S. Moore*†‡§, and John A. Rogers*†‡§¶‖

*Frederick Seitz Materials Research Laboratory, Departments of †Chemistry, ‡Materials Science and Engineering, ¶Mechanical Science and Engineering, and ‖Electrical and Computer Engineering, University of Illinois at Urbana-Champaign, Urbana, IL 61801

Edited by Uwe Bunz, Carnegie Mellon University, and accepted by the Editorial Board March 26, 2008 (received for review October 23, 2007)

Because of their potential for use in advanced electronic, nanomechanical, and other applications, large two-dimensional, carbon-rich networks have become an important target to the scientific community. Current methods for the synthesis of these materials have many limitations including lack of molecular-level control and poor diversity. Here, we present a method for the synthesis of two-dimensional carbon nanomaterials synthesized by Mo- and Cu-catalyzed cross-linking of alkyne-containing self-assembled monolayers on SiO_2 and Si_3N_4. When deposited and cross-linked on flat surfaces, spheres, cylinders, or textured substrates, monolayers take the form of these templates and retain their structure on template removal. These nanomaterials can also be transferred from surface to surface and suspended over cavities without tearing. This approach to the synthesis of monolayer carbon networks greatly expands the chemistry, morphology, and size of carbon films accessible for analysis and device applications.

networks | nanomaterials | self-assembled

In contrast to carbon nanotubes, fullerenes and various derivatives (1–3), the synthesis of large 2D sheets such as graphene (4), graphyne, and graphdiyne (5, 6) extending over micrometers in lateral dimensions is either in its infancy or has significant limitations. In fact, the synthesis of 2D carbon networks has been recognized as an outstanding challenge in materials chemistry (7).

Graphene, the simplest of the 2D conjugated carbon nanomaterials, is produced by micromechanical cleavage of bulk graphite (HOPG) or by thermal decomposition of silicon carbide (8, 9). However, these approaches lack the molecular-level control necessary to define the chemical makeup of these systems. Scholl coupling reactions on oligophenylene precursors (10) produce small (<15 nm) 2D graphene fragments with improved molecular diversity, and radiation induced modifications of self-assembled (11, 12) or Langmuir–Blodgett (13) monolayers create larger sheets, but with reduced control of the chemistry. Polyelectrolytes (14) represent a different class of chemistry that can form 2D (15) and 3D (16) nanomaterials. These films are formed through deposition of separately synthesized polymers, often in layer-by-layer assemblies, in the form of relatively thick (typically >5 nm) films governed by electrostatic interactions. These limitations, together with those associated with the planar, radiation-cross-linked monolayers, motivate the need for alternative approaches to these classes of materials.

A potential solution to the formation of large 2D conjugated carbon nanomaterials would employ a two-step procedure involving the formation of self-assembled monolayers (SAMs) with highly functionalized monomers followed by chemical cross-linkage of the SAMs to form linked monolayers. Fig. 1 shows the overall process beginning with the formation of SAMs of suitably designed carbon precursors on solid supports, followed by chemical cross-linking to yield covalently bonded networks with monolayer thicknesses. Not only could these materials adopt the geometry of the support, but they could also be transferred by using printing-like techniques to other substrates or lithographically patterned into desired geometries. This article introduces the use of synthetic organic methods to create linked carbon monolayers and monolayer membranes in forms ranging from planar or structured films and membranes, to spherical coatings, balloons, tubes, and other complex topologies.

Results

Aryl alkynes are attractive monomers for this chemistry because they are a chemically diverse class of molecules that are already highly conjugated, contain primarily carbon by mass, and can be chemically linked through a variety of methods including alkyne metathesis (17), oxidative Cu coupling (18), and Pd-catalyzed cross-coupling (18). Di-functional monomers (**1** and **2**) and a hexa-functional monomer (**3**) were synthesized with triethoxysilyl groups attached by a carbamate group to the aryl core (Fig. 1*B*) [supporting information (SI) *Text*]. SiO_2- or Si_3N_4-coated substrates or quartz/glass slides were immersed in monomer solutions (≈15 mM monomer, ≈10 mM triethylamine, 90–100°C, 24 h, toluene) creating SAMs that exhibited similar advancing contact angles (74–80°) for all three monomers (Table S1). Two different cross-linking chemistries were used to form linked monolayers from these SAMs. Mo(IV)-catalyzed, vacuum-driven alkyne metathesis (17) linked the dipropyne SAMs derived from **1**. Cu-catalyzed Hay-type coupling conditions (18) created linked monolayers from SAMs of monomers **2** and **3**. The advancing contact angles consistently decreased by 6, 11, and 20° for the dipropyne (**1**), diacetylene (**2**), and terphenyl (**3**) chemistries, respectively. After exposing the SAMs to the linkage conditions, it was found that very little residual metal remained on the substrate.

UV-visible (UV-vis) absorption spectra of the SAMs on UV-grade fused quartz closely matched spectral features of the monomers in solution (Fig. S1). The linked monolayer of **1** on quartz possesses a new shoulder at 330 nm (Fig. 2*A*). Because this new shoulder is small it suggests incomplete polymerization or the formation of oligomers (19, 20). Similarly, the linked monolayer from **2** on quartz possesses a broad new peak at 370 nm (Fig. 2*D*) that matches the absorbance of poly(1,4-phenylene-1,3-butadiynylene) derivatives (20, 21). This has been described as a delocalized $\pi \rightarrow \pi^*$ transition in molecules comprised of multiple 1,4-diphenylbutadiyne chromophores (20). The appearance of these lower-energy peaks suggests an increased delocalization of electrons on oligomerization/polymerization resulting from increased conjugation (21). The spectrum of the linked monolayer of **3** is

Author contributions: M.J.S. and X.Z. contributed equally to this work; M.J.S., X.Z., J.S.M., and J.A.R. designed research; M.J.S., X.Z., S.U., D.-Y.K., Q.C., C.W., and C.L. performed research; X.Z., S.M., J.A.N.T.S., and I.P. contributed new reagents/analytic tools; M.J.S., X.Z., S.U., J.S.M., and J.A.R. analyzed data; and M.J.S., X.Z., J.S.M., and J.A.R. wrote the paper.

Conflict of interest statement: A patent has been filed on this work.

This article is a PNAS Direct Submission. U.B. is a guest editor invited by the Editorial Board.

§To whom correspondence may be addressed. E-mail: moore@scs.uiuc.edu or jrogers@uiuc.edu.

This article contains supporting information online at www.pnas.org/cgi/content/full/0710081105/DCSupplemental.

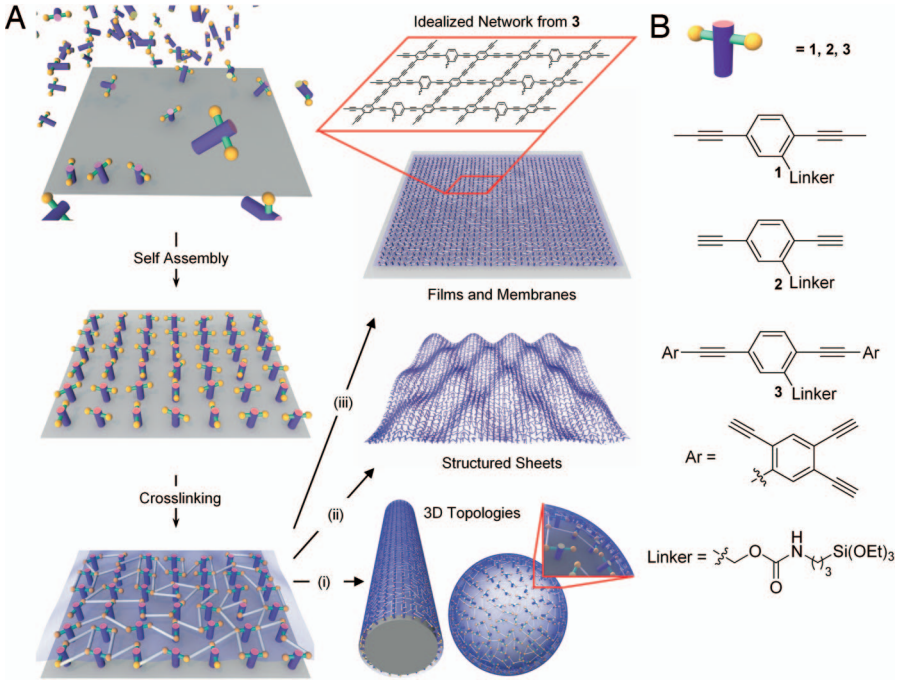

Fig. 1. Schematic illustration of linked monolayer formation. (*A*) Self-assembled monolayers (SAMs) are synthesized on a substrate, then cross-linked to form linked monolayers. This approach is applied to the formation of 3D topologies (*i*), structured sheets (*ii*), and membranes (*iii*). The box above *iii* provides an idealized view of the chemical structure for a linked monomer network formed from monomer 3. (*B*) Chemical structures of monomers 1–3.

significantly broadened compared with that of the original SAM (Fig. S2). No polymers have been synthesized previously from monomers structurally similar to **3**, but the broadening of the absorbance spectra is likely a result of the extensive cross-linking that is possible with this monomer (for an idealized network, see Fig. 1).

Methanol suspensions of SAMs of diacetylene (**2**) coated on 330-nm nonporous SiO_2 spheres exhibit dramatic changes in fluorescence emission on conversion to linked monolayers. A SAM from **2** primarily has a large emission at 315 nm ($\lambda^{ex} = 275$ nm; Fig. 2*E*, blue curves) similar to that of the monomer in solution (Figs. S3–S5). On cross-linking, the emission at 315 nm ($\lambda^{ex} = 275$ nm) weakened significantly and a new emission appeared at 405 nm when excited at 370 nm (Fig. 2*E*, red curves).

Raman spectroscopy provided a convenient means to determine the conversion of SAM **2** to a linked monolayer. Raman spectra of SAM **2** on SiO_2(300 nm)/Si showed a peak at 2,101 cm^{-1}, corresponding to the C≡C stretching mode in terminal phenyl acetylenes (Fig. 2*F*) (22, 23). On exposure of the SAM to cross-linking conditions, the peak at 2,101 cm^{-1} shifts to 2,204 cm^{-1} corresponding to the C≡C stretching mode in phenyl diacetylene (24, 25). The disappearance of the peak from the terminal phenyl acetylene indicates nearly complete conversion of the monomers in the SAM to the corresponding linked monolayer. A variety of conjugated polymers have been previously synthesized that resemble these linked monolayers (20, 21, 26, 27). The spectroscopic changes observed in the monolayer-supported systems are similar to those seen in the literature examples. However, direct comparisons are difficult because the electronics of these polymers are significantly different and very few examples of poly(1,4-phenylene-1,3-butadiynylene) exist (similar to linked SAMs of **2** and **3**). Collectively, the changes in the UV-vis, fluorescence, and Raman spectra provide strong evidence that the SAMs undergo the desired reaction to form linked carbon monolayers Figs. S6 and S7).

In addition to spectroscopic measurements, SAMs and linked monolayers were patterned into 5-μm lines/5-μm space by simple oxygen-reactive ion etching through a layer of photoresist patterned by photolithography. By atomic force micrographs (AFMs), the linked monolayers formed from **1** exhibited only a slight increase in film thickness compared with their SAM precursors (e.g., 1.1–1.4 nm; Fig. 2 *B* and *C*). MM2 molecular geometry optimization of **1** gives a monomer height of ≈1.5 nm, depending on the torsion angle of the aryl rings. The SAM and linked monolayer thicknesses are also similar to those measured for other related system of similar molecular sizes (13, 28). These data indicate that the unlinked and linked SAMs consist of single layers of monomers aligned approximately perpendicular to the surface. The small increase in thickness on cross-linking may be caused by either a change in the orientation of the benzene rings or by the increased average roughness (0.18–0.27 nm). AFM measurements on patterned linked monolayers from **2** and **3** indicate similarly small increases in thickness of 0.5 and 0.3 nm, respectively, relative to their SAMs (Figs. S8–S10). Unlike the films associated with **1**, for which only monolayers form, SAMs from **2** and **3** form multilayers (2.8 and 4.7 nm, respectively) presumably by thermal polymerization during deposition of these reactive multifunctional monomers.

To illustrate the versatility of this approach, we describe methods to release the linked monolayers from their growth substrate and transfer the resulting monolayer membrane to other substrates. These film manipulations made it possible to examine the structural integrity of the monolayer membranes and compare their behavior with the corresponding SAMs. To accomplish this, photoresist is uniformly spin cast onto the SAMs or linked monolayers followed by patterning if desired, and liftoff by selective etching of the support (i.e., bulk SiO_2 or thin films of SiO_2 or Si_3N_4 on other materials) with concentrated HF. The photoresist/SAM or photoresist/monolayer membrane hybrid films are transferred to other substrates and sonicated in acetone to remove the photoresist.

Spectroscopic measurements were performed to examine the possibility of chemical changes in the transferred film induced by exposure to HF, liftoff, and transfer. The UV/vis spectrum of the

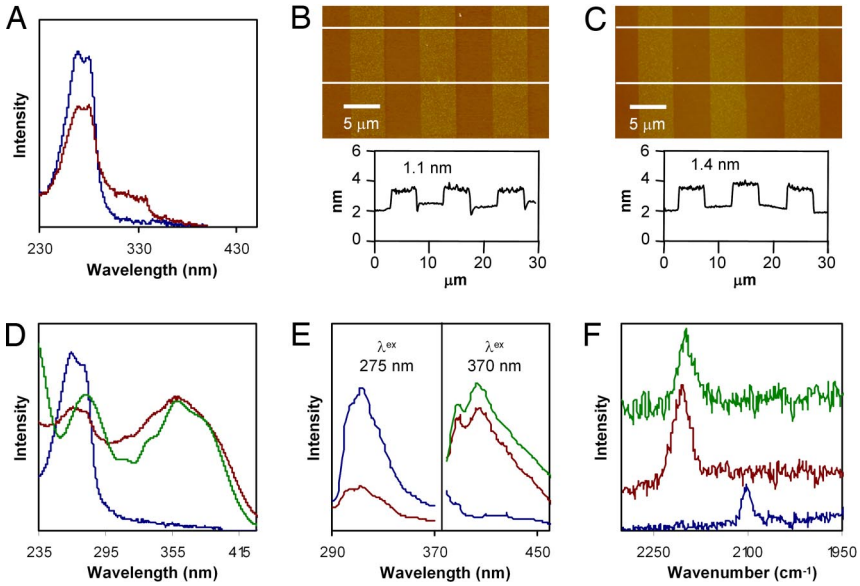

Fig. 2. Spectroscopic data and AFMs of SAMs, linked monolayers, and transferred monolayer membranes. (*A*) Absorption spectra of a SAM (blue), a linked monolayer (red), from **1** on quartz. (*B* and *C*) Tapping-mode AFM of a SAM and a linked monolayer, respectively, from **1** patterned into stripes by photolithography and oxygen-reactive ion etching. The averaged line cuts show a step height of 1.1 nm for the SAM and 1.4 nm for the linked monolayer. (*D*) Absorption spectra of a SAM (blue), a linked monolayer (red), and a transferred monolayer membrane (green) from **2** on quartz. (*E*) Fluorescence spectra (λ^{ex} = 275 nm, *Left*; λ^{ex} = 370 nm, *Right*) of a SAM (blue curves), a linked monolayer (red curves), and an etched monolayer membrane from **2** (green curve) on 330-nm-diameter SiO_2 spheres. Peak heights were normalized to the 315-nm emission of the SAM from **2**. (*F*) Raman spectra of a SAM (blue), linked monolayer (red), and transferred monolayer membranes on a Si wafer with 300 nm thermal SiO_2 (green) from **2**.

monolayer membrane from **2** transferred to a UV grade quartz slide reveals a small shift of the absorbance peak at 275 nm, but the absorption of poly(1,4-phenylene-1,3-butadiynylene) chromophores at 365 nm remains unchanged (Fig. 2*D*, green curve). When the monolayer membrane from **2** grown on silicon oxide beads were etched with aqueous HF, the fluorescence spectra (Fig. 2*E*, green curve) showed a slight increase in intensity, but no change in the overall peak signature (λ^{ex} = 370 nm). Finally, when a sample of monolayer membrane from **2** was transferred to a Si wafer with 300 nm thermal SiO_2, no change in the Raman peak at 2,204 cm^{-1}, corresponding to the C≡C stretching mode in diphenyl diacetylene, was observed (Fig. 2*F*, green curve). Together, these results suggest that the chemical nature of the monolayer membrane remains unchanged after HF etching and transfer.

We explored the modulus and structural integrity in two different types of experiments. First, the transfer of narrow ribbons of monolayer membranes to prestrained elastomeric substrates of poly(dimethylsiloxane) (PDMS) was studied. Releasing the prestrain leads to a nonlinear buckling instability that produces a one-dimensional, sinusoidal pattern of relief. Fig. 3*A* shows AFM images of a ribbon of a monolayer membrane from **2** before and after releasing the prestrain. This type of buckling response will only occur in ribbons of material with high levels of structural integrity and moduli that are much higher than the PDMS (29). Quantitative analysis of the buckling wavelength, with the known modulus of the PDMS (30) and the measured thickness of the monolayer membrane, yielded moduli between 1 and 10 GPa. These values are typical of polymers of similar materials. They are lower than single crystals of dicarbazolyl polydiacetylene (45 GPa) (31) and of graphene (≈1 TPa) (32). Second, to examine the structural integrity and barrier properties of SAMs, linked monolayers, and transferred monolayer membranes, we used wet etching based chemical amplification (33) to evaluate the area density of defects in the films. The defect densities in linked monolayers on their growth substrates [Si (100) with a native oxide layer] are 1.6×10^3, 1.4×10^3, and 9.1×10^2 defects per mm^2 for **1**, **2**, and **3**, respectively (Fig. 3*B Inset*). Several factors could contribute to the density of defects in the linked monolayers, such as defects on growth surfaces, defects in SAMs formation, and defects as a result of polymer shrinkage. Although polymer shrinkage may be an issue, especially for molecule **3**, it is challenging to assess its influence without information on packing density during the SAM formation. In particular, if the initial SAMs are packed very tightly, cross-linkage may actually result in expansion instead of shrinkage. The densities in linked monolayers are ≈10 times lower than those of the corresponding SAMs, suggesting a linking mechanism that tends to eliminate defects. The defect densities in the linked monolayers are, in fact, only slightly higher than well developed alkanethiolate SAMs on gold (33), which are known to have much better order and quality than SAMs of silanes. Similar studies performed on a monolayer membrane from **2** transferred to a substrate of Au(200 nm)/Cr(5 nm)/SiO_2(300 nm)/Si indicated a ≈10-fold increase in defect density compared with the same linked monolayer on its growth substrate (Fig. 3*A*). This increase is due, at least in part, to slight mechanical damage during transfer. Release of stresses associated with polymerization shrinkage could also contribute.

Although monolayer films are invisible on most substrates, we found that these transferred monolayer membranes could be visualized directly under an optical microscope when supported by oxidized Si substrates with an oxide layer of 300 nm, similar to observations in single-layer graphene (8). The Si wafer with 300 nm thermal SiO_2 was selected because the phase contrast between the monolayer membrane and the wafer results in a shift from violet-blue to blue (34). For all transferred films, we observed flat, continuous films largely free of defects over areas of several square millimeters (Fig. 3*C*). Near their edges, these monolayer membranes exhibited folds, holes, and tears, which we attribute to the transfer process.

The transferred monolayer membranes were also analyzed by AFM and transmission electron microscopy (TEM). A folded region of a transferred film from **1** showed clear correlations

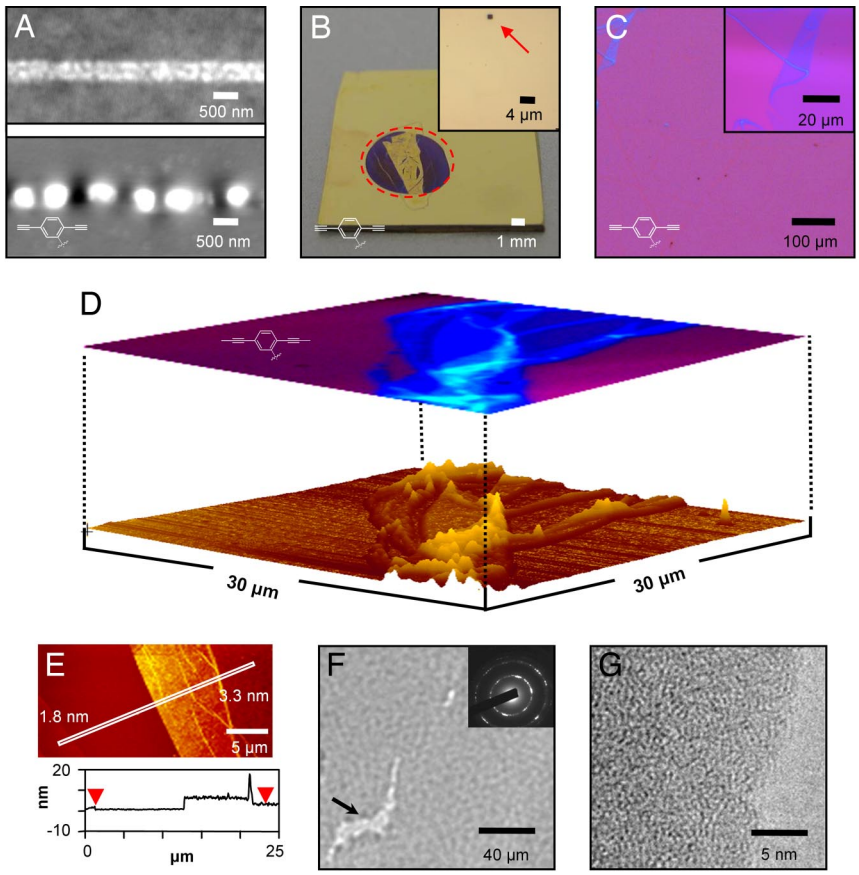

Fig. 3. Characterization of transferred monolayer membranes. (*A*) AFM images of a ribbon of a monolayer membrane from **2** (width = 500 nm) on a prestrained PDMS substrate before *(Upper)* and after (*Lower*) releasing the prestrain. (*B*) Image of a sample of monolayer membrane from **2** transferred to a substrate of Au(200 nm)/Cr(5 nm)/SiO_2(300 nm)/Si after wet etching the Au with a ferricyanide solution in a circular region (dashed line) surrounding the membrane. The etched areas appear as dark blue; the unetched gold region in the center corresponds to the transferred monolayer membranes. (*Inset*) An optical micrograph of a silicon substrate that supports a linked monolayer, collected after exposure to KOH etchant. The arrow indicates an etched pit corresponding to a pinhole defect in the monolayer. (*C*) Reflection mode optical micrograph of a monolayer membrane from **2** transferred to a Si wafer with a 300-nm thermal SiO_2 layer. (*Inset*) High-magnification micrograph of folds in the film. (*D*) Reflectance optical micrograph superimposed on tapping-mode AFM image of a monolayer membrane from **1** transferred to a Si wafer with a 300-nm thermal SiO_2 layer. (*E*) Tapping-mode AFM image and line-cut height profile showing a monolayer membrane from **1** with regions of 1.8- and 3.3-nm height, consistent with folding on transfer to a Si wafer with a 300-nm thermal SiO_2 layer. (*F*) Low-magnification TEM image of a monolayer membrane from **1** transferred to a holey carbon-coated grid. The arrow points toward a small defect in the film created by the transfer process. (*Inset*) An electron diffraction pattern with rings at 1.1 Å and 2 Å, but otherwise no significant in-plane ordering. (*G*) High-magnification TEM image of a monolayer membrane from 1 transferred to holey carbon-coated grid showing a film largely free of pinhole defects.

between thickness determined by tapping-mode AFM and intensity of the optical micrograph (Fig. 3*D*). The transferred monolayer membrane from **1** has a slightly increased thickness (1.8 nm) that likely results from a layer of water between the film and SiO_2 surface (8). Additionally, a folded area has a thickness (3.3 nm) that is approximately twice the nominal thickness for the rest of the film (Fig. 3*E*). The folding ability of these nanometer-thick films is a testament of their mechanical strength. TEM images of a monolayer membrane from **1** transferred to a holey carbon grid revealed a tightly packed monolayer with uniform thickness and very few pinhole defects that may have been invisible using AFM (Fig. 3 *F* and *G*).

The low density of defects and the high structural integrity of the linked monolayers allowed the creation of more exotic film geometries. Transfer of a monolayer membrane from **1** onto a substrate with an array of cylindrical holes (≈440 nm diameter, ≈400 nm depth) produces suspended monolayer "drumheads" that were nondestructively imaged by AFM and scanning electronic microscopy (SEM; Fig. 4 *A* and *B*). Again, the absence of torn regions illustrates the remarkable mechanical robustness of these systems.

The ability to form linked monolayers on a wide range of planar, nonplanar, or three-dimensional substrates creates further opportunities for fabrication of unusual structures. For example, a linked monolayer from **1** was formed directly on a substrate with an array of shallow voids (≈35 nm), to produce a continuous linked monolayer in the form of a 2D "pleated sheet" (Fig. 4 *C* and *D*). On transfer of the membrane, the AFM power spectrum shows an in-plane periodicity of the "pleats" that matches that of the growth substrate. However, the relief is only ≈1.2 nm, as might be expected from partial or complete folding of the monolayer membrane in the regions corresponding to the edges of relief in the substrate.

This strategy also allowed the formation of linked monolayers on 3D objects as well. SAMs of **1** were deposited on 226 ± 16 nm nonporous SiO_2 spheres with a procedure similar to that used for flat substrates. After linking, the SiO_2 substrate was removed by HF vapor etching to yield empty monolayer membrane "balloons." Fig. 4 shows TEM images of monolayer-coated spheres (Fig. 4*E*) and balloons (Fig. 4*F*). Histograms created from observation of many such objects show a close correspondence between sphere and balloon diameters, but the balloons

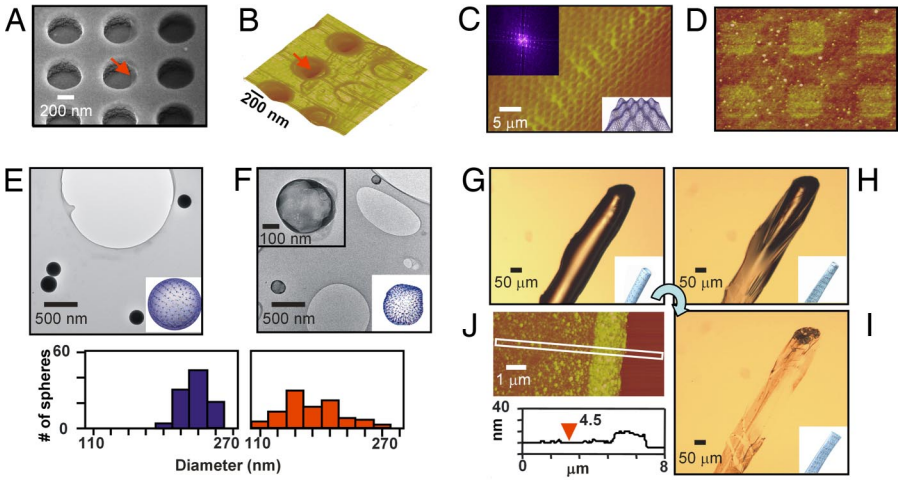

Fig. 4. Images of ''unusual'' monolayer membrane structures. (*A* and *B*) SEM and AFM images, respectively, of a membrane from **1** transferred onto a substrate with a square array of cylindrical holes (diameters ≈440 nm and depths ≈400 nm) to form ''drumhead'' structures. Red arrows point to the same region of the film that is suspended over the edge of a hole. (*C* and *D*) AFM and high-resolution AFM images, respectively, of a monolayer membrane from **1** grown on a substrate similar to that in *A*, but with relief depths of ≈35 nm, and then transferred to a flat Si wafer with a 300-nm thermal SiO_2 layer. (*C Inset Upper Left*) Power spectrum of the AFM image, indicating a well defined periodicity consistent with that of the growth substrate. (*C Inset Lower Right*) Illustration of a ''pleated sheet.'' (*E* and *F*) TEM images and diameter distributions of a monolayer membrane from **1** deposited on SiO_2 spheres imaged on a holey carbon-coated grid before (*E*) and after (*F*) HF vapor etching of the SiO_2. *Insets* are illustrations of the imaged structures. (*G–I*) Time-resolved reflection mode optical micrographs of a tubular membrane from **3** filled with HF/water immediately after HF vapor etching of optical fiber, after 20 min open to the air, and after complete drying, respectively. *Insets* are illustrations of the imaged structures. (*J*) AFM image of this collapsed tube. The line scan corresponds to an average over the area indicated by the rectangle.

have a slightly wider distribution and smaller size (diameters, 168 ± 32 nm) because of partial collapse on removal of the silica support. A similar process was carried out with ≈125-μm-diameter optical fibers by using SAMs of **3**. Immediately after the HF vapor etch, water droplets were observed within the hollow fibers. Fig. 4 *G*, *H*, and *I* show time-sequential optical micrographs illustrating evaporation of this encapsulated water. The AFM image in Fig. 4*J* shows that the monolayer membrane that remains after drying is consistent with the nominal layer thickness (≈4.5 nm center thickness), although capillary forces induced by the contracting HF/water droplet may be responsible for large nonuniformities near the edges. In a saturated environment, the water-filled monolayer membrane tubes maintain their shape for hours without tearing, providing additional evidence of their robustness.

A remaining topic of interest involves how the monolayer membranes are being held together. Although it could be envisioned that these membranes are being held together by polysiloxane formation during SAM deposition, transfer of *unlinked* SAMs of **1** and **2** yielded neither films nor film fragments. For the SAM of **3**, film fragments were observed but they were smaller and contained many more defects than the corresponding monolayer membrane. The small fragments in this case likely result from inadvertent cross-linking by air oxidation or by thermal polymerization under the SAM deposition conditions. Additionally, if these membranes were being held together through polysiloxanes it is highly unlikely that they would stand up to treatment with HF. Exposure of SAMs from **1** and **2** to the linkage conditions, yields linear oligomeric/polymer chains. Conceivably, these chains can be held together in a woven network, although this type of geometry is not necessary to explain the structural integrity of the films; previous studies of related systems indicate that purely noncovalent interactions can yield similar properties (13, 35). However, monolayer membranes from **3** are most likely held together because of multiple cross-linking. Both of these proposed mechanisms would explain the mechanical strength of the monolayer membranes on removal of the support and their flexibility to adopt the geometry of the given support.

Discussion

In conclusion, we have shown that linked carbon monolayers can be formed on a variety of solid surfaces. These linked monolayers are synthesized by linking three different alkyne-containing monomers with two different carbon–carbon bond-forming reactions [Mo(IV)-catalyzed alkyne metathesis and Cu-catalyzed Hay coupling]. The linked monolayers synthesized on flat surfaces have extremely large aspect ratios and are easily transferred from the native surface by protecting with photoresist and etching the inorganic substrate. These monolayer membranes are sufficiently robust to be suspended over 440-nm-diameter holes without tearing. The linked monolayers were also prepared on structured surfaces and 3D supports, and the freestanding monolayer membranes maintained the shape of the original support after etching. This approach to the synthesis of monolayer carbon networks provides a powerful method to explore the properties and device applications of a wide variety of carbon films. Other linking chemistries and monomers are currently being explored for the synthesis of conducting, 2D monolayer films.

Materials and Methods

Representative Synthesis of SAMs on Flat Substrates. A freshly cleaned and dried substrate was placed in a reaction vial containing a 0.015 M solution of **1** in toluene and TEA (10 mM) under a nitrogen atmosphere. The vial was sealed and heated to 95–100°C for 24 h. The substrate was removed and rinsed once with toluene, twice with dichloromethane, and sonicated for 5 min in toluene. The rinse was repeated and the substrate was sonicated for 5 min in methanol. The rinse was repeated and the substrate blown dry under a stream of nitrogen.

Synthesis of Linked Monolayers by Alkyne Metathesis. In a glovebox, 5.0 mg of trisamidomolybdenum(IV) propylidyne and 3.3 mg of *p*-nitrophenol were dissolved in 3 ml of trichlorobenzene in a reaction vial. The substrate was added, and the flask was sealed and placed under a vacuum (5 torr) for 22 h. The substrate was removed from the vial and rinsed once with dimethylfor-

mamide (DMF), once with a 0.1 M solution of sodium diethylcarbamodithioate in DMF, once with toluene, twice with dichloromethane, then sonicated in toluene for 5 min. The rinse was repeated and the substrate was sonicated for 5 min in methanol. The rinse was repeated a third time and the substrate was blown dry with a stream of nitrogen.

Synthesis of Linked Monolayers by Copper Coupling. In a reaction vial, 20 mg of CuCl was dissolved in 3 ml of degassed acetone. To this suspension was added 61 μl of TMEDA and the solution was allowed to stir under a nitrogen atmosphere at room temperature for 30 min. At this time, the substrates were added and the reaction vial purged with oxygen from a balloon. The mixture was stirred under an oxygen atmosphere for 15 h. The substrate was removed from the vial and rinsed once with DMF, once with a 0.1 M solution of sodium diethylcarbamodithioate in DMF, once with toluene, twice with dichloromethane, then sonicated in toluene for 5 min. The rinse was repeated and the substrate was sonicated for 5 min in methanol. The rinse was repeated a third time and the substrate was blown dry with a stream of nitrogen.

ACKNOWLEDGMENTS. We thank Prof. J. Notestein, Dr. T. Spila, Dr. R. Haasch, V. Petrova, Tu Truong, Prof. M. Shim, T. Banks, and K. Colravy for helpful discussions and help with analytical facilities. This work was supported by U.S. Department of Energy, Division of Materials Sciences Award DE-FG02-07ER46471, through the Frederick Seitz Materials Research Laboratory. All imaging and surface analysis, supported by Award DE-FG02-91ER45439, was performed at the Frederick Seitz Materials Research Laboratory Center for Microanalysis. S.U. was supported, in part, by the Anandamahidol Foundation.

1. Kroto HW, Heath JR, O'Brien SC, Curl RF, Smalley RE (1985) C_{60}: Buckminsterfullerene. *Nature* 318:162–163.
2. Krätschmer W, Lamb LD, Fostiropoulos K, Huffman DR (1990) Solid C_{60}: A new form of carbon. *Nature* 347:354–358.
3. Lu X, Chen Z (2005) Curved pi-conjugation, aromaticity, and the related chemistry of small fullerenes (C_{60}) and single-walled carbon nanotubes. *Chem Rev* 105:3643–3696.
4. Geim AK, Novoselov KS (2007) The rise of graphene. *Nat Mater* 6:183–191 and references therein.
5. Spitler EL, Johnson CA, II, Haley MM (2006) Renaissance of annulene chemistry. *Chem Rev* 106:5344–5386.
6. Tahara K, Yoshimura T, Sonoda M, Tobe Y, Williams RV (2007) Theoretical studies on graphyne substructures: Geometry, aromaticity, and electronic properties of the multiply fused dehydrobenzo[12]annulenes. *J Org Chem* 72:1437–1442.
7. Diederich F, Rubin Y (1992) Synthetic approaches toward molecular and polymeric carbon allotropes. *Angew Chem Int Ed* 31:1101–1123.
8. Novoselov KS, *et al.* (2004) Electric field effect in atomically thin carbon films. *Science* 306:666–669.
9. Berger C, *et al.* (2006) Electronic confinement and coherence in patterned epitaxial graphene. *Science* 312:1191–1196.
10. Wu J, Pisula W, Müllen K (2007) Graphenes as potential material for electronics. *Chem Rev* 107:718–747.
11. Chechik V, Crooks RM, Stirling CJM (2000) Reactions and reactivity in self-assembled monolayers. *Adv Mater* 12:1161–1171.
12. Eck W, Küller A, Grunze M, Völkel B, Gölzhäuser A (2005) Freestanding nanosheets from cross-linked biphenyl self-assembled monolayers. *Adv Mater* 17:2583–2587.
13. Arias-Marin E, *et al.* (2003) Amphiphilic phenyl-ethynylene polymers and copolymers. Synthesis, characterization, and optical emission properties. *Macromolecules* 36:3570–3579.
14. Decher G (2003) Polyelectrolyte multilayers, an overview. *Multilayer Thin Films*, eds Decher G, Schlenoff JB (Wiley-VCH, Weinheim, Germany), pp 1–46.
15. Rubner MF (2003) pH-Controlled fabrication of polyelectrolyte multilayers: Assembly and applications. *Multilayer Thin Films*, eds Decher G, Schlenoff JB (Wiley-VCH, Weinheim, Germany), pp 133–154.
16. Jiang C, Tsukruk VV (2006) Freestanding nanostructures via layer-by-layer assembly. *Adv Mater* 18:829–840.
17. Zhang W, Moore JS (2007) Alkyne metathesis: Catalysts and synthetic applications. *Adv Synth Catal* 349:93–120.
18. Siemsen P, Livingston RC, Diederich F (2000) Acetylenic coupling: A powerful tool in molecular construction. *Angew Chem Int Ed* 39:2633–2657.
19. Kim I-B, Dunkhorst A, Gilbert J, Bunz UHF (2005) Sensing of lead ions by a carboxylate-substituted PPE: Multivalency effects. *Macromolecules* 38:4560–4562.
20. Pelter A, Jones DE (2000) The preparation and some properties of substituted phenylene-ethynylene and phenylenebuta-1,3-diynylene polymers. *J Chem Soc, Perkin Trans 1* 14:2289–2294.
21. Anand S, *et al.* (2006) Optical excitations in carbon architectures based on dodecadehydrotribenzo[18]annulene. *J Phys Chem A* 110:1305–1318.
22. Patterson ML, Weaver MJ (1985) Surface-enhanced Raman spectroscopy as a probe of adsorbate-surface bonding: simple alkenes and alkynes adsorbed at gold electrodes. *J Phys Chem* 89:5046–5051.
23. Abramczyk H, Waliszewska G, Kolodziejski M (1998) Raman spectra of phenylacetylene in acetonitrile and methylcyclohexane at low temperatures. 2. Structural order and vibrational relaxation in frozen matrices at 77 K. *J Phys Chem A* 102:7765–7771.
24. Schrader B, *et al.* (2005) Non-destructive Raman analyses—Polyacetylenes in plants. *Spectrochim Acta Part A* 61:1395–1401.
25. Meskers SCJ, Peeters E, Langeveld-Voss BMW, Janssen RAJ (2000) Circular polarization of the fluorescence from films of poly(p-phenylene vinylene) and polythiophene with chiral side chains. *Adv Mater* 12:589–594.
26. Hittinger E, Kokil A, Weder C (2004) Synthesis and characterization of cross-linked conjugate polymers milli-, micro-, and nanoparticles. *Angew Chem Int Ed* 43:1808–1811.
27. Kim J, Swager TM (2001) Control of conformational and interpolymer effects in conjugated polymers. *Nature* 411:1030–1033.
28. Yam CM, Tong SSY, Kakkar AK (1998) Simple acid-base hydrolytic chemistry approach to molecular self-assembly: thin films of long chain alcohols terminated with alkyl, phenyl, and acetylene groups on inorganic oxides surfaces. *Langmuir* 14:6941–6947.
29. Khang D-Y, Jiang H, Huang Y, Rogers JA (2006) A stretchable form of single-crystal silicon for high-performance electronics on rubber substrates. *Science* 311:208–212.
30. Wilder EA, Guo S, Lin-Gibson S, Fasolka MJ, Stafford CM (2006) Measuring the modulus of soft polymer networks via a buckling-based metrology. *Macromolecules* 39:4138–4143.
31. Galiotis C, *et al.* (1984) High-modulus polydiacetylene single-crystal fibers. *J Polym Sci Polym Phys Ed* 22:1589–1606.
32. Bunch JS, *et al.* (2007) Electromechanical resonators from graphene sheets. *Science* 315:490–493.
33. Zhao X-M, Wilbur JL, Whitesides GM (1996) Using two-stage chemical amplification to determine the density of defects in self-assembled monolayers of alkanethiolates on gold. *Langmuir* 12:3257–3264.
34. Henrie J, Kellis S, Schultz SM, Hawkins A (2004) Electronic color charts for dielectric films on silicon. *Opt Express* 12:1464–1469.
35. Day D, Lando JB (1980) Morphology of crystalline diacetylene monolayers polymerized at the gas-water interface. *Macromolecules* 13:1478–1483.